nature metabolism

LETTERS

https://doi.org/10.1038/s42255-019-0151-7

A biosensor for measuring NAD$^+$ levels at the point of care

Qiuliyang Yu[1,2], Narges Pourmandi[1], Lin Xue[1], Corentin Gondrand[1], Sebastian Fabritz[1], Daniel Bardy[3], Luc Patiny[2], Elena Katsyuba[4,5], Johan Auwerx[4] and Kai Johnsson[1,2*]

The cellular level of nicotinamide adenine dinucleotide (NAD$^+$), through its different functions, affects cellular metabolism and signalling[1–3]. A decrease in the NAD$^+$ content has been associated with various pathologies and physiological aging[4,5], while strategies to boost cellular NAD$^+$ levels have been shown to be effective against age-related diseases in many animal models[6]. The link between decreased NAD$^+$ levels and numerous pathologies and physiological aging has triggered the need for a simple quantification method for NAD$^+$, ideally applicable at the point of care. Here, we introduce a bioluminescent biosensor for the rapid quantification of NAD$^+$ levels in biological samples, which can be used either in laboratories or at the point of care. The biosensor is a semisynthetic, light-emitting sensor protein that changes the colour of emitted light from blue to red on binding of NAD$^+$. This NAD$^+$-dependent colour change enables the use of the biosensor in paper-based assays in which NAD$^+$ is quantified by measuring the colour of the emitted light by using either a simple digital camera or a plate reader. We used the approach to quantify NAD$^+$ levels in cell culture, tissue and blood samples, yielding results that agreed with those from standard testing methods. The same biosensor furthermore allows the quantification of NAD$^+$-dependent enzymatic activities in blood samples, thus expanding its utility as a tool for point-of-care diagnostics.

At present, NAD$^+$ levels are routinely measured by liquid chromatography coupled to mass spectrometry (LC–MS)[7] or enzymatic assays[8]. However, both methods are time-consuming and labour-intensive, and they require expensive equipment, making them unsuitable for point-of-care applications. To address these limitations, we developed a biosensor for the quantification of NAD$^+$ at the point of care. The biosensor design (Fig. 1a) was based on our previously reported approach for developing semisynthetic, bioluminescent sensors[9], and the finding that fluorescent derivatives of the drug sulfamethoxazole bind to the dehydrogenase sepiapterin reductase (SPR) in an NAD$^+$-dependent manner[10]. To exploit this feature for the generation of our biosensor, we expressed a fusion protein (NAD-Luc, Fig. 1a) comprising SPR, the luciferase NanoLuc (NLuc) and the self-labelling protein SNAP-tag[11], and we labelled the SNAP-tag with a fluorescent sulfamethoxazole derivative (Fig. 1a). According to our design, the tethered sulfamethoxazole derivative should bind to SPR in the presence of NAD$^+$. This would bring the fluorophore Cy3 into close proximity with the luciferase NLuc and should enable bioluminescence resonance energy transfer (BRET) from NLuc to Cy3. In the absence of NAD$^+$, there is no binding of the tethered sulfamethoxazole and very little BRET should occur. Therefore, the ratio between the emission intensities of the luciferase and the fluorophore (NLuc/Cy3) would be controlled by the concentration of NAD$^+$. As a result, recording of the ratio of NLuc/Cy3 permits the quantification of the analyte NAD$^+$ independently of the sensor concentration and the signal intensity, thus making NAD-Luc a bioluminescent sensor that directly measures NAD$^+$. The titration of our biosensor NAD-Luc with NAD$^+$ indeed revealed a 170 ± 13% change in the emission ratio NLuc/Cy3 and a c_{50} value of 13.1 ± 1.2 μM (Fig. 1b). The c_{50} value represents the NAD$^+$ concentration at which the sensor is at 50% of its maximal ratio change. The c_{50} is controlled by the apparent affinity of the sensor for NAD$^+$ as well as its BRET efficiency under the experimental conditions (Supplementary Table 1). To increase the magnitude of the observed ratio change, we replaced NLuc with a circular permutated NLuc (cpNLuc)[9], in which new termini were created near the active site of the luciferase (Extended Data Fig. 1). We assumed that this would shorten the distance between the ligand-binding site of SPR and the active site of the luciferase, thereby increasing the BRET efficiency in the closed state of the sensor. The resulting sensor NAD-cpLuc indeed showed an improved maximum ratio change of 650 ± 26% and a c_{50} of 2.7 ± 0.3 μM (Fig. 1b,c). Further, we attempted to increase the sensitivity of the sensor for NAD$^+$. Previous experiments and sequence comparisons with SPR homologues identified a number of residues (position 17, 41 and 42) in the active site of SPR that are critical for its affinity and selectivity towards NAD$^+$ (Extended Data Fig. 2)[10]. To identify mutants with an increased affinity for NAD$^+$, we performed saturation mutagenesis at positions 17, 41 and 42 and screened the resulting sensor libraries for variants with an increased affinity for NAD$^+$. The screening led to NAD-cpLuc^2 with the following mutations in SPR: R17K, A41D and R42L, which showed a tenfold lower c_{50} (0.27 ± 0.02 μM) relative to NAD-cpLuc, while conserving the large ratio change (Fig. 1b). Similarly to NAD-cpLuc, NAD-cpLuc^2 showed a high specificity for NAD$^+$ over related molecules, such as NADH, NADP$^+$, NADPH and the biosynthetic precursors of NAD$^+$ (Extended Data Fig. 3). Together, NAD-cpLuc and NAD-cpLuc^2 cover a range of NAD$^+$ concentrations from about 10^{-8} M to 10^{-4} M. To validate the design principle of our sensor, we tested its modularity by replacing either SNAP-tag with HaloTag[12], another self-labelling protein, or NanoLuc with TurboLuc[13], another coelenterazine-utilizing luciferase. The resulting sensors showed dynamic ranges and sensitivities that are comparable to NAD-cpLuc (Extended Data Fig. 4), which validated the underlying design principle.

[1]Department of Chemical Biology, Max Planck Institute for Medical Research, Heidelberg, Germany. [2]Institute of Chemical Sciences and Engineering, École Polytechnique Fédérale de Lausanne (EPFL), Lausanne, Switzerland. [3]Clinical Chemistry Laboratory, Service of Biomedicine, University Hospital of Lausanne, Lausanne, Switzerland. [4]Laboratory of Integrative Systems Physiology, Faculty of Life Sciences, École Polytechnique Fédérale de Lausanne (EPFL), Lausanne, Switzerland. [5]Present address: Nagi Biosciences, Lausanne, Switzerland. *e-mail: johnsson@mr.mpg.de

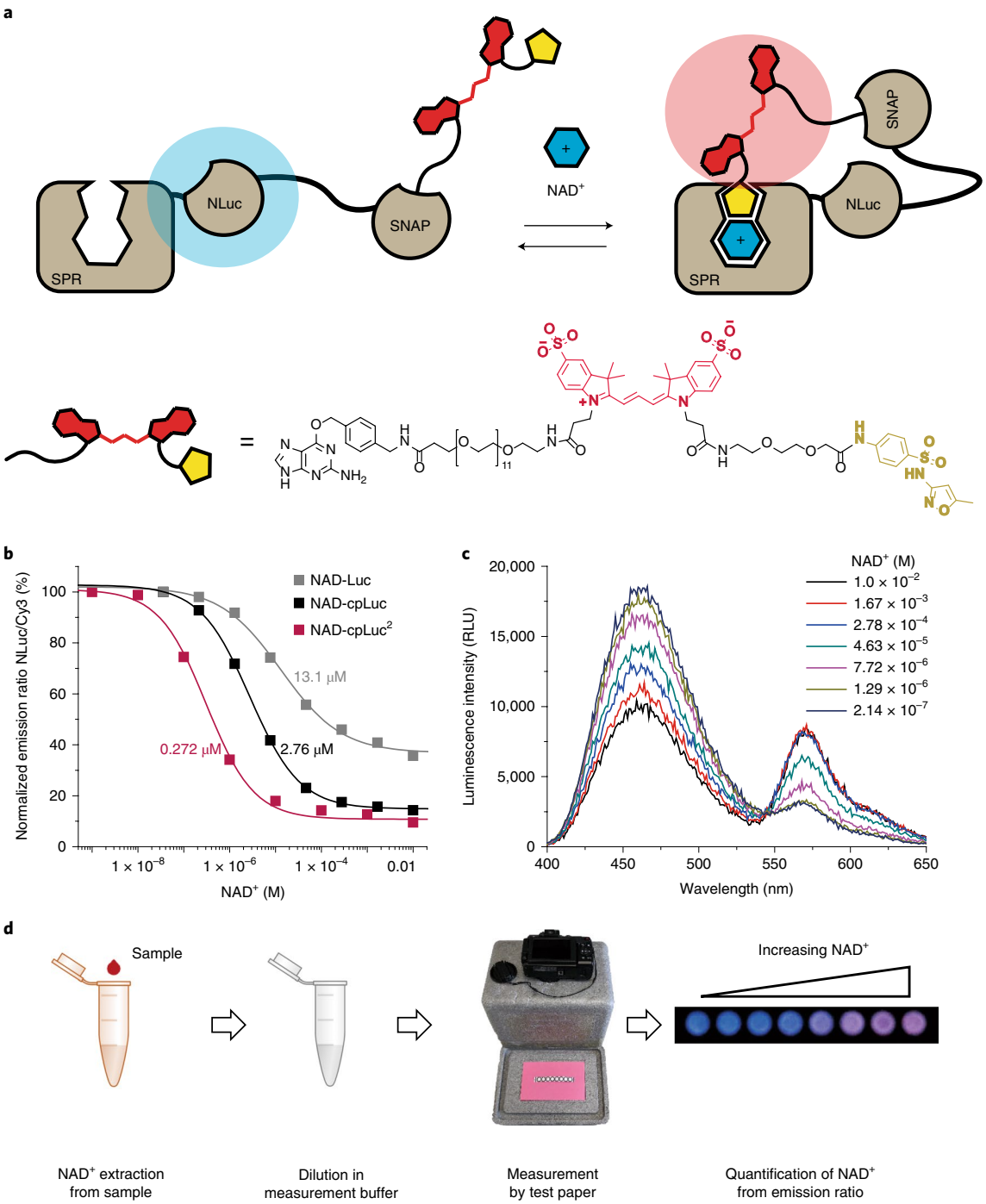

Fig. 1 | NAD⁺ sensor and assay design. a, Scheme of the NAD⁺ sensing mechanism and structure of the tethered ligand comprising benzylguanine as substrate of a SNAP-tag (black), Cy3 fluorophore (red) and sulfamethoxazole (yellow) ligand for SPR. **b**, Titration curves of sensor variants. The normalized emission ratio (NLuc/Cy3) was plotted as a function of NAD⁺ concentrations. **c**, Emission spectra of NAD-cpLuc at different NAD⁺ concentrations. **d**, Flow diagram of NAD⁺ paper assay using a digital camera for readout. The plots shown in **b** and **c** were repeated three times independently with similar results.

We have previously shown that BRET-based biosensors are well suited for paper-based assays at the point of care[9,14]. In this assay format, the sensor protein is lyophilized on paper and is resolubilized on addition of processed samples. The readout can be performed by a microplate reader or a simple digital camera (Fig. 1d)[9]. In addition to its simplicity, this assay format also reduces matrix effects: as the sample is spread out as a thin layer, the emitted light travels only a short distance through the sample and intersample differences in concentrations of light-absorbing molecules, such as bilirubin, do not distort the measured emission ratio. Furthermore, only 5 µl of the processed sample needs to be applied onto the test paper, which minimizes the consumption of biological samples. As a first test, we quantified NAD⁺ concentrations in lysates of HEK293 cells and compared the results with those obtained by LC–MS. In these experiments, the cells were cultured under three different conditions: (1) under normal DMEM; (2) in the presence

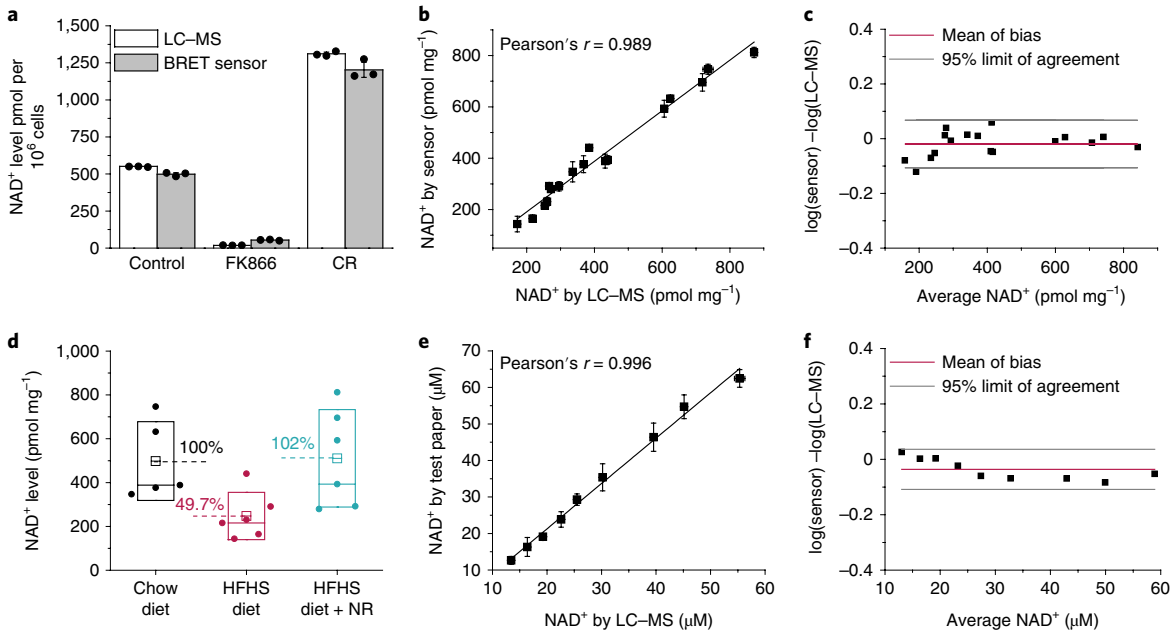

Fig. 2 | NAD⁺ sensor performance in paper-based assays. a, Cell lysate NAD⁺ measurement from HEK293 cells cultured under control conditions, FK866 treatment and caloric restriction (CR). **b**, Comparison between hepatic NAD⁺ measurement by sensor and LC–MS from C57BL/6J male mouse liver samples. Different hepatic NAD⁺ levels were induced by feeding mice with different diets for 18 weeks. **c**, Bland–Altman analysis of hepatic NAD⁺ measurement in the mice described in **b**. **d**, Hepatic NAD⁺ measurement presented according to treatment groups: normal chow diet ($n=5$), HFHS diet ($n=6$) or HFHS diet supplemented with NR (400 mg kg^{-1} d^{-1}) ($n=6$) for 18 weeks. Individual dot: average of three independent measurements by NAD⁺ sensor for each sample. Box: s.d. from each group. White square: mean from each group. Percentages: relative NAD⁺ levels considering the mean of NAD⁺ level from chow diet group as 100%. **e**, Whole-blood NAD⁺ measurement in commercially available human blood samples. The results obtained by LC–MS were used as reference. **f**, Bland–Altman analysis of blood NAD⁺ measurement. All samples were processed to extract NAD⁺ and diluted before the measurement. Values in **a**,**b** and **e** are given as means ± s.d. for $n=3$ independent measurements. Values in **c** and **f** are given as means of $n=3$ independent measurements.

of FK866, an inhibitor of nicotinamide phosphoribosyltransferase that reduces the cellular NAD⁺ level;[15] or (3) under conditions that mimic caloric restriction, which results in an increase in the cellular NAD⁺ level[16,17]. The cells were lysed in 75% buffered ethanol and the samples were cleared by centrifugation, a step that is required for analysis by LC–MS, but not for the NAD⁺ sensor (Extended Data Fig. 5). For analysis using NAD-cpLuc², extracts were diluted tenfold in a buffer containing the luciferase substrate furimazine, and 5 µl of the mixture were spotted onto a test paper containing lyophilized NAD-cpLuc². The emission ratios (NLuc/Cy3) were measured by a luminescent plate reader and were converted into NAD⁺ concentrations by using a calibration curve. Relative to the control, the caloric restriction resulted in a more than twofold increase in the NAD⁺ content, while the incubation with FK866 decreased the NAD⁺ levels by one order of magnitude (Fig. 2a). In the control and the calorie-restricted samples, the values measured through LC–MS and NAD-cpLuc² were within 15% error (549 ± 2 pmol per 10^6 cells and 498 ± 11 pmol per 10^6 cells for the control samples, and 1,310 ± 13 pmol per 10^6 cells and 1,203 ± 51 pmol per 10^6 cells for the calorie-restricted samples). As for the FK866 treatment group, both methods indicated very low NAD⁺ levels (18.4 ± 0.5 pmol per 10^6 cells for LC–MS and 54.0 ± 3.1 pmol per 10^6 cells for NAD-cpLuc²), even though the two methods showed larger relative differences at this low concentration range.

Tissue NAD⁺ levels have been analysed in many animal metabolic studies. A fast and accurate detection method that consumes a small amount of sample and requires minimal sample handling would greatly facilitate such studies. We therefore used NAD-cpLuc² to quantify NAD⁺ levels in tissue samples. We analysed homogenized liver samples from C57BL/6J male mice kept under three different dietary conditions: (1) regular chow diet, (2) high-fat, high-sucrose (HFHS) diet and (3) HFHS diet complemented with the NAD⁺ precursor, nicotinamide riboside (NR). It has been shown previously that mice under HFHS diet have lower hepatic NAD⁺ levels, but that NR administration can bring these levels back to normal[18]. After extraction of homogenized liver samples with buffered ethanol, the extracts were analysed by LC–MS and NAD-cpLuc². The results from the two methods correlated very well, with a Pearson's r of 0.989 (Fig. 2b) and the agreement between the two methods was also confirmed by Bland–Altman analysis (Fig. 2c). The analysis of the samples using NAD-cpLuc² furthermore confirmed that the hepatic NAD⁺ levels of mice on HFHS diet are significantly decreased relative to the chow diet, and that NR as a food supplement raised the hepatic NAD⁺ levels back to normal (Fig. 2d). Theoretically, only 0.1 mg of sample is required to perform the test paper measurement. Practically, on average, 5 mg of liver samples were used to ensure precise weighting of the sample.

Raising cellular NAD⁺ levels is a promising strategy for maintaining and improving health[2,3]. Such strategies can be based on administrating biosynthetic precursors of NAD⁺, such as NR, or practising caloric restriction. Studies have shown that their impact on the whole-blood NAD⁺ levels can be substantial: oral administration of NR to a human study participant raised basal blood NAD⁺ levels from around 20 µM to 50 µM, as determined by LC–MS[7]. The possibility to monitor NAD⁺ levels at the point of care, either in a hospital setting or by patients themselves, would greatly facilitate the development of strategies to raise cellular NAD⁺ levels and aid in the evaluation of the medical efficacy of such strategies. To test whether NAD-cpLuc² could be used to quantify whole-blood NAD⁺ levels, we analysed commercial blood spiked with various concentrations of NAD⁺. The whole-blood samples were diluted fourfold in 75% buffered ethanol for cell lysis, after which the samples were cleared

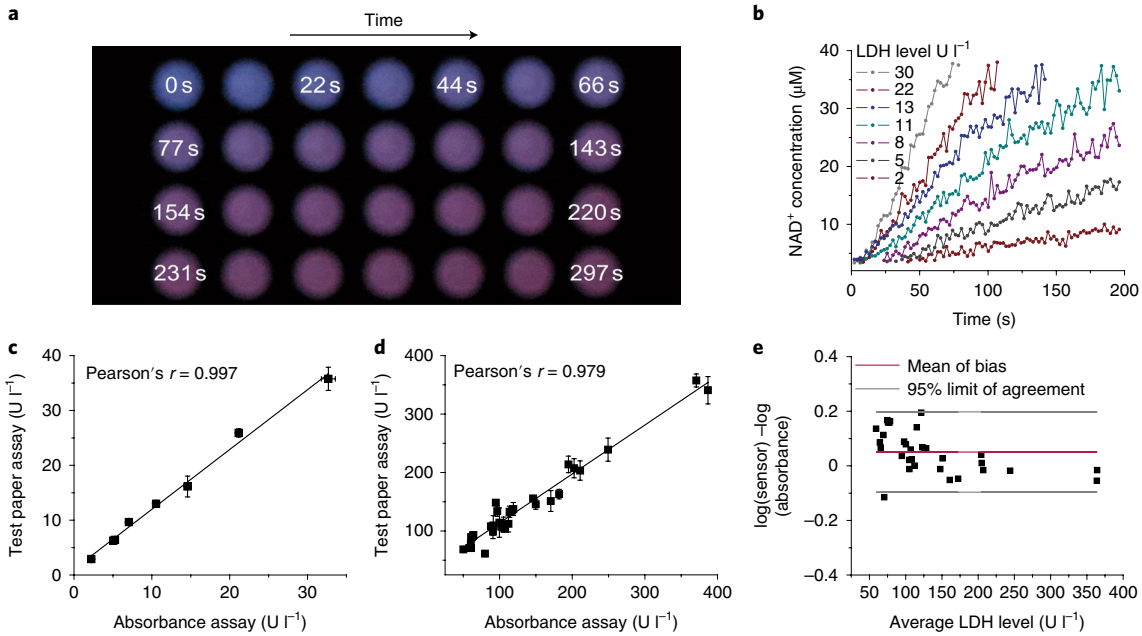

Fig. 3 | NAD⁺ sensor for kinetic measurements. a, Photographs captured at different time points of NAD⁺ kinetic measurement on test paper. NAD⁺ was produced over time by the enzymatic reaction, making the sensor close and emit red light. **b**, Kinetic measurement of NAD⁺ production for quantifying LDH activity. NAD⁺ concentrations were plotted as a function of time. The plots shown in **a** and **b** were repeated three times independently with similar results. **c**, Test paper quantification of LDH spiked in serum. The results obtained by absorbance assay were used as reference. **d**, Test paper quantification of LDH in patient samples. The results obtained by absorbance assay were used as reference. **e**, Bland–Altman analysis of patient sample LDH quantification. Values in **c** and **d** are given as means ± s.d. for $n = 3$ independent measurements. Values in **e** are given as means of $n = 3$ independent measurements.

through centrifugation. The centrifugation was required for the analysis using LC–MS, but could be omitted for the NAD⁺ test paper (Extended Data Fig. 5). Then, the supernatant was measured by both the test paper and LC–MS. For the test paper analysis, the sample was diluted tenfold in a buffer containing furimazine. This solution (5 µl) was spotted on a test paper containing lyophilized NAD-cpLuc[2] and analysed using a digital camera. Without the centrifugation step, the whole procedure takes less than 5 min. The results obtained by NAD-cpLuc[2] and LC–MS showed excellent correlation, with a Pearson's $r = 0.996$ (Fig. 2e) and the agreement of the two methods was confirmed by Bland–Altman analysis (Fig. 2f). We have also shown that the test paper can be stored for more than 40 d at ambient temperature without an apparent decrease in performance (Extended Data Fig. 8). The quantification of whole-blood NAD⁺ levels with a simple camera and test paper at the point of care should facilitate studies on the role of NAD⁺ levels in physiological aging and in various pathologies. At present, the manual dilution steps still prevent patients from completing self-testing, but the development of a more automated version of this assay should be possible.

An important feature of our biosensor is that it does not consume NAD⁺. Therefore, it should be suitable for the continuous monitoring of NAD⁺ in enzymatic assays at the point of care, given that the formation or consumption of NAD⁺ is slower than the closing or opening of the biosensor[10]. We therefore investigated its use for determining enzymatic activities in blood samples. A clinically relevant application would be quantifying plasma levels of lactate dehydrogenase (LDH), which is an indicator of tissue damage and is routinely measured in clinical laboratories, for example, during anticancer treatments[19]. To determine LDH levels, we measured the formation rate of NAD⁺ during the LDH-catalysed reduction of pyruvate to lactate[20]. Specifically, we lyophilized pyruvate together with NAD-cpLuc on the test paper. The sample is then diluted in a reaction buffer that contains NADH and furimazine, so that the reaction only starts after addition of the diluted sample to the test paper. We used NAD-cpLuc in these experiments because its low NAD⁺ sensitivity prevents a too fast saturation of the sensor under the assay conditions. To perform the assay, we diluted commercial plasma spiked with various concentrations of LDH in a reaction buffer containing furimazine and NADH, spotted it on the test paper and analysed it by taking photographs every 2.8 s (Fig. 3a) for 5 min, during which the sample evaporation was minimal (Extended Data Fig. 6). Plotting the resulting NAD⁺ concentrations as a function of time (Fig. 3b) yielded the LDH levels (Fig. 3c). The LDH levels measured by the test paper and a conventional absorbance assay showed excellent correlation (Pearson's $r = 0.997$) (Fig. 3c). We further validated the approach by analysing 32 plasma samples from patients, which again demonstrated a good agreement between the test paper and the absorbance assay, with a Pearson's r of 0.979 (Fig. 3d,e). Moreover, to demonstrate the generality of the approach, we successfully established similar quantitative assays for alanine aminotransferase (ALT) and aspartate aminotransferase (AST) (Extended Data Fig. 7, Supplementary Table 2), which are two other clinically relevant biomarkers for liver function assessment[21]. These experiments demonstrate how the continuous measurement of NAD⁺ concentrations in paper-based assays could be exploited for running metabolic assays at the point of care. Furthermore, the NAD⁺ sensor complements our previously introduced BRET sensor for NADPH[9]. Together, these two sensors establish a broad platform for running metabolic assays at the point of care.

In summary, we introduce a bioluminescent biosensor for the direct quantification of NAD⁺. Using paper-based assays, the biosensor enables the rapid determination of NAD⁺ levels in cellular and tissue samples, and can be performed in laboratories or at the point of care. We expect that the biosensor will greatly facilitate studies on the role of cellular NAD⁺ levels in physiological aging and in numerous pathologies.

Methods

Sensor production. A functional sensor consists of a recombinant sensor protein and a synthetic tether. The recombinant sensor protein was cloned in a pET51b$^+$ plasmid and expressed in *Escherichia coli* strain BL21(DE3). The SPR variant used for the generation of the sensors NAD-Luc and NAD-cpLuc contains the mutations A41D and R42W, to switch the cofactor sensitivity from NADP to NAD$^+$ (ref. [10]). The *E. coli* was cultured in 1 l LB medium containing 50 μg ml^{-1} ampicillin with shaking at 220 r.p.m. and 37 °C to reach an optical density of 0.6 at 600 nm. Then the culture was cooled down to 16 °C and isopropyl β-D-thiogalactopyranoside (IPTG) was added (0.5 mM) to induce overnight protein expression. The bacterial culture was then centrifuged at 4,000*g* for 10 min and lysed by sonication in the presence of 1 μg ml^{-1} lysozyme and 1 mM phenylmethyl sulfonyl fluoride. The lysate was sequentially loaded onto Ni-NTA (Qiagen) and Strep-Tactin (IBA) columns for purification. The purified protein was concentrated using protein spin columns with a cut-off of 50 kDa. The synthetic tether was prepared following the procedure described in the Supplementary Methods. Functional BRET sensors were formed by incubating 8 μM synthetic tether with 2 μM fusion protein in a buffer containing 50 mM HEPES and 50 mM NaCl at pH 7.2 at room temperature for 1 h. The resulting sensors were used without further purification.

BRET sensor characterization. The functional BRET sensors were titrated with NAD$^+$, NADH, NADP$^+$, NADPH, nicotinic acid adenine dinucleotide, nicotinamide mononucleotide and nicotinamide to assess their sensitivity and selectivity. Various concentrations of the cofactors were mixed with 500 pM sensor and 1,000-fold diluted furimazine (Nano-Glo Luciferase Assay Substrate, Promega) in 100 μl of buffer (50 mM HEPES, 50 mM NaCl, pH 7.2) in a white 96-well plate (PerkinElmer). Bioluminescence was measured using a Tecan Spark 20M plate reader (Tecan) with NLuc emission measured at 458 nm (bandwidth 15 nm) and Cy3 emission measured at 578 nm (bandwidth 15 nm). The ratios between NLuc and Cy3 emission (NLuc/Cy3) were plotted against the cofactor concentrations. The sensor's open ratio (R_o), closed ratio (R_c), c_{50} and Hill coefficient (h) were obtained by fitting the data to the Hill–Langmuir equation (equation (1)).

$$R = R_o - \frac{R_o - R_c}{1 + \left(\frac{c_{50}}{[\text{cofactor}]}\right)^h} \quad (1)$$

The c_{50} value represents the NAD$^+$ concentration at which the sensor is at 50% of its maximal ratio change. The c_{50} is related to the K_D for NAD$^+$ by the following equation:

$$c_{50} = [K_D(P_{o2}/P_{c2})]^{1/h} \quad (2)$$

where P_{o2} is a proportionality coefficient relating concentration of open sensor to measured emission intensity at 570 nm and P_{c2} is a proportionality coefficient relating concentration of closed sensor to measured emission intensity at 570 nm. The relation between c_{50} and K_D values is derived in the Supplementary Methods.

Generation of protein libraries. The library pET51b$^+$ plasmid with ampicillin resistance that encodes saturating mutations on a specific site was prepared using degenerated primers. The degenerated primers were mixed with a ratio of NDT:VHG:TGG = 12:9:1. The plasmid library was prepared using standard PCR and Gibson assembly. The purified library plasmid was sequenced to verify incorporation of the degenerated codons. Then, the *E. coli* strain BL21(DE3) was transformed with the plasmid library and was spread out on LB agar plates containing 100 μg ml^{-1} ampicillin. After an overnight incubation at 37 °C, single colonies were inoculated into 2-ml 96-deep-well plates containing 400 μl LB medium with 50 μg ml^{-1} ampicillin. The bacterial cultures were incubated at 37 °C for 4 h with 500 r.p.m. shaking rate. Then, 50 μl of the culture were transferred to 2-ml 96-deep-well plates containing 950 μl LB medium with 50 μg ml ampicillin and was incubated at 37 °C for 6 h with 500 r.p.m. shaking rate. The rest of the culture was spun down and stored at 4 °C. To induce protein expression, 1,000 μl of each of the bacterial cultures was first incubated at 16 °C for 1 h with 500 r.p.m. shaking rate and then supplied with IPTG (0.5 mM). The resulting culture was further incubated at 16 °C overnight with 500 r.p.m. shaking rate. The bacteria were then collected by centrifugation at 5,000*g* for 15 min. The bacteria pellet was frozen and thawed for two cycles before being lysed using 300 μl of a lysis buffer (50 mM K_2HPO_4, pH 8) containing 1 mg ml^{-1} lysozyme and 2 mM $MgCl_2$ at 37 °C for 1 h. The cell debris resulting from the lysis was separated from the supernatant by centrifugation at 5,000*g* for 20 min. The cleared supernatant was transferred into clean 96-well plates for characterization.

Screening of protein libraries using bioluminescent readout. The screening aims to identify the variants with an improved NAD$^+$ sensitivity. The library supernatant containing the protein variants was incubated with the tethered fluorescent ligand at a concentration of 2 μM for 1 h at room temperature. The labelled supernatant (2 μl) was added into 98 μl of buffer (50 mM HEPES, 50 mM NaCl, pH 7.2) containing various concentrations of NAD$^+$ and the 1,000-fold diluted NLuc substrate furimazine. The bioluminescent emission spectrum from each variant was then recorded using a Tecan Spark 20M plate reader (Tecan). The ratios between NLuc and Cy3 emission (NLuc/Cy3) were plotted versus the cofactor concentrations to assess the sensor's sensitivity. The bacterial cultures of the most sensitive variants were amplified to obtain their plasmids. The purified plasmids were sequenced. Sensor proteins were purified from 1-l bacteria cultures and were characterized as described above to confirm the result.

Test paper preparation and stability test. The NAD$^+$ test papers were prepared through paper printing, BSA blocking and sensor lyophilization on cellulose-based chromatography paper (Whatman no.1, GE Healthcare). The printing of black circles on the chromatography paper to define the testing area was performed using a solid ink printer (Xerox ColorQube 8580N). The printed test paper was heated at 90 °C for 10 min. After cooling to room temperature, 5 μl of aqueous solution containing 10 mg ml^{-1} BSA and 0.2% TWEEN 20 (v/v) was added onto the test paper for blocking. Then, 5 μl of buffer containing the sensor and reagents for enzymatic reactions was lyophilized on the paper. The test papers for measuring NAD$^+$ from biological samples contained 0.5 pmol of labelled NAD-cpLuc[2] in lyophilized form. The test papers for enzymatic activities contained 0.5 pmol of labelled NAD-cpLuc. The components for test paper blocking and sensor lyophilization are summarized in Supplementary Table 2. The functional test papers were stored at room temperature in the dark. The stability of the test paper containing NAD-cpLuc was assessed by titration using samples with known NAD$^+$ concentrations over a period of 42 d. The total luminescent intensity, R_o, R_c and c_{50} were measured to evaluate the test paper stability.

Sample preparation. NAD$^+$ in biological samples to be quantified by the BRET sensor and LC–MS was extracted by lysing samples using buffered ethanol. Samples were lysed by a thorough mixing with 4 volumes of the lysis buffer containing 75% ethanol and 25% HEPES buffer (50 mM HEPES, 50 mM NaCl, pH 7.2). The mixture was further vortexed for 2 min. The cell debris and protein aggregates were separated by centrifugation at 10,000*g* for 10 min at 4 °C. For analysis by the BRET sensor, the supernatant was further diluted tenfold in a measurement buffer (50 mM HEPES, 50 mM NaCl, pH 7.2) containing 100-fold diluted furimazine. For analysis by MS, the supernatant was diluted 1,000-fold in a 2 mM ammonium acetate buffer (pH 9). Samples for analysis by MS were mixed with an equal volume of reconstituted internal standard (^{13}C-labelled yeast extract) before lysis.

In vitro measurement of NAD$^+$ using test paper and LC–MS. The cell culture samples were prepared by culturing HEK293 cells in T-75 boxes to confluency in DMEM with 10% FBS. The cells were then either treated with 100 nM of FK886 or changed to calorie restriction medium (2.5 mM D-glucose + 10 mM 2-deoxyglucose). After incubation for 24 h at 37 °C, 70% humidity and 5% CO_2, the cells were counted, and 3×10^6 cells were collected by centrifugation. The cell pellets were then lysed and analysed by the test paper and LC–MS as described above.

The liver samples came from wild-type male C57BL/6J mice (Charles River Laboratories) maintained on normal chow diet or high-fat high-sucrose diet (Harlan Laboratories, TD.08811, 45% kcal fat diet) starting from 8 weeks of age, for 18 weeks. The NR-treated group received 400 mg kg^{-1} d^{-1} dose of NR in their high-fat sucrose diet pellets starting from 8 weeks of age for 18 weeks. The animals were housed under a 14-h light, 10-h dark cycle at 21–23 °C, with ad libitum access to water and food during the experiment. Animals were then separated into different diet groups at the age of 8 weeks for the 18-week experiment[18]. No littermate control was used during the experiment. The homogenized samples were thawed, lysed and measured using the test paper and LC–MS as described below. Liver tissues contain relatively high levels of alcohol dehydrogenase (ADH)[22]. To test whether, in the presence of ADH, the use of ethanol in the extraction buffer leads to a major reduction in NAD$^+$, we performed a control experiment in which ADH (purified from *Saccharomyces cerevisiae*, Sigma Aldrich, 1 U ml^{-1}) was mixed with NAD$^+$ (15 μM) and the solution was mixed with 4 volumes of buffered ethanol with or without the ADH inhibitor 4-methylpyrazole hydrochloride (50 mM). The samples were then analysed by the BRET sensor as described. Using the current sample treatment method, no less than 80% of NAD$^+$ was preserved (Extended Data Fig. 9).

The blood samples spiked with NAD$^+$ were obtained by adding NAD$^+$ in commercially available single human donor whole blood purchased from Innovative Research with Na_2EDTA as anticoagulant. The spiked samples were prepared by weighting NAD$^+$ powder and diluting freshly prepared stock solutions. The spiked NAD$^+$ concentrations were 60.0 μM, 50.0 μM, 41.7 μM, 34.7 μM, 28.9 μM, 24.1 μM, 20.1 μM, 16.7 μM and 14.0 μM. The samples were treated with buffered ethanol as described above. The background NAD$^+$ level of the commercial blood was analysed by LC–MS and was found to be 0.15 ± 0.03 μM. We assume that the low background level resulted from the long storage of the commercial blood.

For all biological samples, 5 μl of the solution resulting from the ethanol extraction and the dilution in measurement buffer was added onto the test paper containing NAD-cpLuc[2] for measurement using a PowerShot G1X camera (Canon) or a Tecan Spark 20M plate reader (Tecan). The following settings were used for the camera measurement: focus, 20 cm; ISO, 6,400; exposure time, 1.3 s;

file format, JPEG. The photographs captured by the camera were further analysed by a previously described open source script[14]. The script recognizes the bright spots and extracts the blue and red intensities. The emission ratio was obtained by dividing the blue intensity by the red intensity. The ratio was used to calculate the NAD^+ concentration on the basis of a titration curve obtained under the same conditions. The measurement began 5 s after spotting the samples onto the test paper.

The NAD^+ concentration was calculated on the basis of a titration curve. The titration was performed by measuring the emission ratios with known concentrations of NAD^+ spiked in a buffer composed of 10% lysis buffer and 90% measurement buffer. The NAD^+ concentrations in unknown samples were calculated using the rearranged Hill–Langmuir equation (equation (3))

$$[\text{cofactor}] = c_{50}\left(\frac{R_o - R}{R - R_c}\right)^{1/h} \quad (3)$$

In parallel, the samples were analysed by LC–MS. A Shimadzu Nexera UPLC system hyphenated to a Sciex QTrap 6500+ triple-quadrupole mass spectrometer was used for the LC–MS analysis. The Sciex's Analyst v.1.6.3 software controlled the instruments. Freshly prepared sample (6 µl), as described above, was injected on an Acquity UPLC HSS T3 (Waters, 2.1 × 50 mm², 1.8 µm) column. The column temperature was set to 30 °C. The analytes were eluted using a 350 µl min^{-1} flow of an aqueous 2.5 mM NH_4OAc solution (pH 6) and acetonitrile (both ultra LC–MS grade). After sample injection, a 2-min isocratic flow of 100% of the aqueous phase was applied, followed by a 0 to 25% organic phase gradient. Subsequently, the column was washed using 98% acetonitrile and re-equilibrated, resulting in an overall analysis time of 10 min per sample. NAD^+ and its internal standard featured a retention time of 4.5 min. For MS analysis positive and negative polarity electrospray ionization were investigated. Albeit the absolute signal intensities for NAD^+ were higher in positive mode, ionization was performed in negative mode due to the better signal to noise ratio. For NAD^+ ionization under the described high-flow conditions the following ion source parameters were chosen: curtain gas 40 psi, collision gas 'high', ionization voltage −4,500 V, temperature 400 °C, heater gas 65 psi and nebulizer gas 80 psi. MS/MS analysis was performed in the multireaction monitoring (MRM) mode. The following MRM transitions were used: NAD1 661.9→540.0 *m/z* (declustering potential −35 V, collision energy −20 V, cell exit potential −35 V), NAD2 661.9→ 79.0 *m/z* (declustering potential −35 V, collision energy −130 V, cell exit potential −35 V), NAD-^{13}C-IS 683.0→555.0 *m/z* (declustering potential −35 V, collision energy −20 V, cell exit potential −35 V). For the quantification of the MRM signals a solvent calibration curve covering a concentration range from 0.5 to 250 ng ml^{-1} in nine steps was used. The quantitative data analysis was performed with Sciex's MultiQuant v.3.0.2 software. Integration of the MRM traces was performed after the application of a 1-point Gaussian smooth. The resulting areas were internal standard corrected and a linear (weighting 1/*x*) regression ($r = 0.999$) was applied. Instrument reproducibility was tested via five injections of the 10 ng ml^{-1} NAD^+ standard (percentage coefficient of variation, <3%).

Measurement of enzyme kinetics using test paper and other reference methods. The enzyme level in the plasma is represented by the NAD^+ production rate in the corresponding enzymatic reactions. LDH levels can be determined by either measuring the rate of oxidation of lactate or the reduction of pyruvate; most laboratories currently measure the oxidation of lactate by recording the formation of NADH[20]. We chose to measure the formation of NAD^+ for two practical reasons. First, measuring the rate of oxidation of lactate ideally requires saturating concentrations of NAD^+, which would saturate our sensor protein. Second, the relative changes in NAD^+ concentrations are much larger when measuring its formation instead of its consumption. The LDH assay was performed by diluting the plasma sample 20-fold in a reaction buffer (50 mM HEPES, 50 mM NaCl, pH 7.2) containing NADH and furimazine, 5 µl of which was further added onto the test paper containing 0.5 pmol of NAD^+ sensor and 25 nmol of pyruvate. The ALT assay was performed by diluting the plasma sample 20-fold in a reaction buffer (50 mM HEPES, 50 mM NaCl, pH 7.2) containing 500 mM alanine, lactate dehydrogenase, 150 µM NADH and furimazine, 5 µl of which was further added onto the test paper containing 0.5 pmol of NAD^+ sensor and 75 nmol of 2-oxoglutarate. The AST assay was performed by diluting the plasma sample 20-fold in a reaction buffer (50 mM HEPES, 50 mM NaCl, pH 7.2) containing 240 mM aspartate, lactate dehydrogenase, malate dehydrogenase, 150 µM NADH and furimazine, which was further added onto the test paper containing 0.5 pmol of NAD^+ sensor and 60 nmol of 2-oxooglutarate. To obtain the NAD^+ production rate, we used the test paper and digital camera to measure the NAD^+ concentrations as described above, which were also plotted versus the time. The production rate was then calculated from the slope obtained through linear regression. In parallel, absorbance spectrometry was used to measure the enzymatic levels in the plasma. Instead of measuring the NAD^+ production rate, this method measures the NADH consumption rate in the reaction by following its absorbance at 340 nm. The LDH assay was performed by diluting the plasma sample 20-fold in a buffer (50 mM HEPES, 50 mM NaCl, pH 7.2) containing 5 mM pyruvate and 150 µM NADH. The LDH samples from patients were obtained from University Hospital of Lausanne, Service of Biomedicine, Clinical Chemistry Laboratory. The samples were flash-frozen for storage and were thawed at room temperature before measurement. The ALT assay was performed by diluting the ALT-spiked plasma 20-fold in a buffer (50 mM HEPES, 50 mM NaCl, pH 7.2) containing 15 mM 2-oxoglutarate, 500 mM alanine, 150 µM NADH and 2 µM lactate dehydrogenase. The AST assay was performed by diluting the AST-spiked plasma sample 20-fold in a buffer (50 mM HEPES, 50 mM NaCl, pH 7.2) containing 12 mM 2-oxoglutarate, 240 mM aspartate, 150 µM NADH, 2 µM lactate dehydrogenase and 2 µM malate dehydrogenase. To obtain the NADH consumption rate, an absorbance spectrometer was used to measure the NADH concentrations in the samples on the basis of its extinction coefficient, which was further plotted versus the time. The NADH consumption rate was then calculated from the slope obtained through linear regression of the curve.

Reporting Summary. Further information on research design is available in the Nature Research Reporting Summary linked to this article.

Data availability

The data that support the findings of this study are available from the corresponding author upon request. Source data for Figs. 1–3 and Extended Data Figs. 3–9 are provided with the paper. Plasmids of the sensors are available on AddGene through No.135627 (NAD-Luc), 135628 (NAD-cpLuc) and 135629 (NAD-cpLuc[2]).

Received: 18 April 2019; Accepted: 12 November 2019;
Published online: 13 December 2019

References

1. Belenky, P., Bogan, K. L. & Brenner, C. NAD^+ metabolism in health and disease. *Trends Biochem. Sci.* **32**, 12–19 (2007).
2. Canto, C., Menzies, K. J. & Auwerx, J. NAD^+ metabolism and the control of energy homeostasis: a balancing act between mitochondria and the nucleus. *Cell Metab.* **22**, 31–53 (2015).
3. Fang, E. F. et al. NAD^+ in aging: molecular mechanisms and translational implications. *Trends Mol. Med.* **23**, 899–916 (2017).
4. Rajman, L., Chwalek, K. & Sinclair, D. A. Therapeutic potential of NAD-boosting molecules: the in vivo evidence. *Cell Metab.* **27**, 529–547 (2018).
5. Katsyuba, E. & Auwerx, J. Modulating NAD^+ metabolism, from bench to bedside. *EMBO J.* **36**, 2670–2683 (2017).
6. Yoshino, J., Baur, J. A. & Imai, S. I. NAD^+ intermediates: the biology and therapeutic potential of NMN and NR. *Cell Metabol.* **27**, 513–528 (2018).
7. Trammell, S. A. J. et al. Nicotinamide riboside is uniquely and orally bioavailable in mice and humans. *Nat Commun* **7**, 12948 (2016).
8. Karp, M. T., Raunio, R. P. & Lövgren, T. N. Simultaneous extraction and combined bioluminescent assay of NAD+ and NADH. *Anal Biochem.* **128**, 175–180 (1983).
9. Yu, Q. et al. Semisynthetic sensor proteins enable metabolic assays at the point of care. *Science* **361**, 1122–1126 (2018).
10. Sallin, O. et al. Semisynthetic biosensors for mapping cellular concentrations of nicotinamide adenine dinucleotides. *eLife* **7**, e32638 (2018).
11. Keppler, A. et al. A general method for the covalent labeling of fusion proteins with small molecules in vivo. *Nat Biotechnol* **21**, 86–89 (2003).
12. Los, G. V. et al. HaloTag: a novel protein labeling technology for cell imaging and protein analysis. *ACS Chem. Biol.* **3**, 373–382 (2008).
13. Auld, D. S. et al. Characterization and use of TurboLuc luciferase as a reporter for high-throughput assays. *Biochemistry* **57**, 4700–4706 (2018).
14. Griss, R. et al. Bioluminescent sensor proteins for point-of-care therapeutic drug monitoring. *Nat. Chem. Biol.* **10**, 598–603 (2014).
15. Hasmann, M. & Schemainda, I. FK866, a highly specific noncompetitive inhibitor of nicotinamide phosphoribosyltransferase, represents a novel mechanism for induction of tumor cell apoptosis. *Cancer Res.* **63**, 7436–7442 (2003).
16. Wood, J. G. et al. Sirtuin activators mimic caloric restriction and delay ageing in metazoans. *Nature* **430**, 686–689 (2004).
17. Chen, D. et al. Tissue-specific regulation of SIRT1 by calorie restriction. *Genes Dev.* **22**, 1753–1757 (2008).
18. Gariani, K. et al. Eliciting the mitochondrial unfolded protein response by nicotinamide adenine dinucleotide repletion reverses fatty liver disease in mice. *Hepatology* **63**, 1190–1204 (2016).
19. Extermann, M. et al. Predicting the risk of chemotherapy toxicity in older patients: the Chemotherapy Risk Assessment Scale for High-Age Patients (CRASH) score. *Cancer* **118**, 3377–3386 (2012).
20. Vanderlinde, R. E. Measurement of total lactate dehydrogenase activity. *Ann. Clin. Lab. Sci.* **15**, 13–31 (1985).
21. Pollock, N. R. et al. A paper-based multiplexed transaminase test for low-cost, point-of-care liver function testing. *Sci. Transl. Med.* **4**, 152ra129 (2012).
22. Algar, E. M., Seeley, T. L. & Holmes, R. S. Purification and molecular properties of mouse alcohol dehydrogenase isozymes. *Eur. J. Biochem.* **137**, 139–147 (1983).

Acknowledgements
This work was supported by the Max Planck Society, the Swiss National Science Foundation and EPFL.

Author contributions
Q.Y. and K.J. conceived this study. Q.Y., N.P., L.X., C.G., S.F., D.B., L.P., E.K., J.A. and K.J. performed experiments, provided samples, performed data analysis and contributed to manuscript writing.

Competing interests
K.J. is inventor on a patent application filed by EPFL. Patent number: US10221439B2; Sensors, methods and kits for detecting nicotinamide adenine dinucleotides. J.A. is a consultant to Mitobridge. All other authors declare no conflict of interest.

Additional information
Extended data is available for this paper at https://doi.org/10.1038/s42255-019-0151-7.

Supplementary information is available for this paper at https://doi.org/10.1038/s42255-019-0151-7.

Correspondence and requests for materials should be addressed to K.J.

Peer review information Primary Handling Editor(s): Ana Mateus; Christoph Schmitt.

Reprints and permissions information is available at www.nature.com/reprints.

Publisher's note Springer Nature remains neutral with regard to jurisdictional claims in published maps and institutional affiliations.

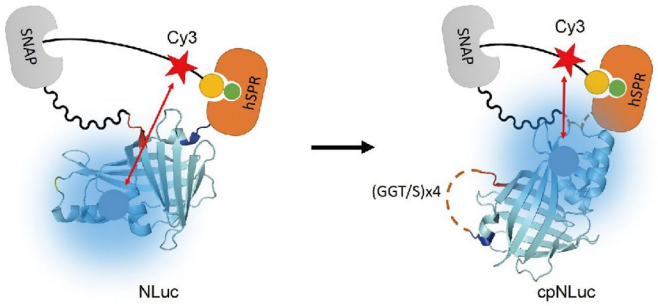

Extended Data Fig. 1 | Improving sensor performance using cpNLuc. The distance between the active site (glowing blue ball) and the fluorophore Cy3 is shortened when using cpNLuc as the BRET donor, resulting in a higher energy transfer efficiency in the closed state of the sensor.

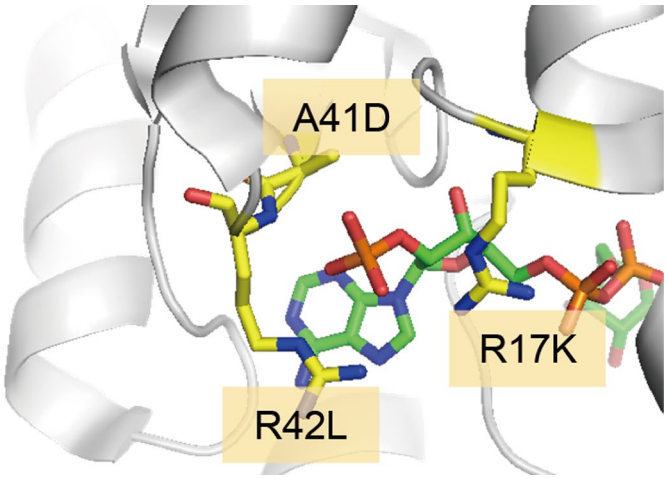

Extended Data Fig. 2 | Cofactor binding site of wild-type hSPR. Residues contributing to cofactor binding and randomized for improving NAD^+ binding affinity of the BRET sensor are highlighted in yellow. The selected mutant NAD-cpLuc[2] carries the SPR mutation A41D, R42L and R17K. The SPR used for the generation of sensor NAD-Luc and NAD-cpLuc contains the mutation A41D and R42W to switch the cofactor sensitivity from $NADP^+$ to NAD^+. SPR PDB ID = 4HWK.

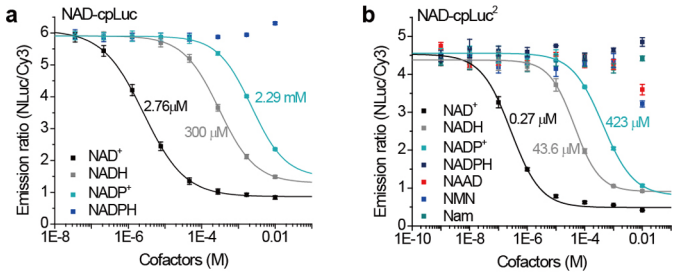

Extended Data Fig. 3 | Titration of NAD-cpLuc and NAD-cpLuc². Titration curve of **a**, NAD-cpLuc and **b**, NAD-cpLuc² with various cofactors and biosynthetic precursors of NAD^+. Error bars represent ± SD of n = 3 independent measurements.

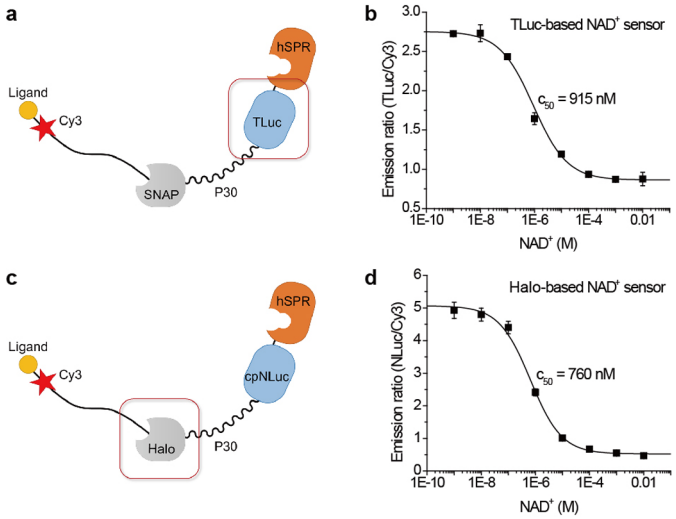

Extended Data Fig. 4 | Modularity of BRET sensor components. a, Cartoon of the sensor using TLuc as BRET donor. **b**, Performance of the sensor using TLuc as BRET donor. The resulting sensor showed a smaller signal response compared to the cpNLuc-based sensor. **c**, Cartoon of the sensor using HaloTag (Halo) as the self-labeling protein. **d**, Performance of the sensor using HaloTag for attaching fluorescent sulfamethoxazole derivative *Halo-PEG11-Cy3-SMX*. The structure of *Halo-PEG11-Cy3-SMX* and its synthesis is described in the section "SYNTHESIS OF COMPOUNDS". Error bars represent ± SD of n = 3 independent measurements.

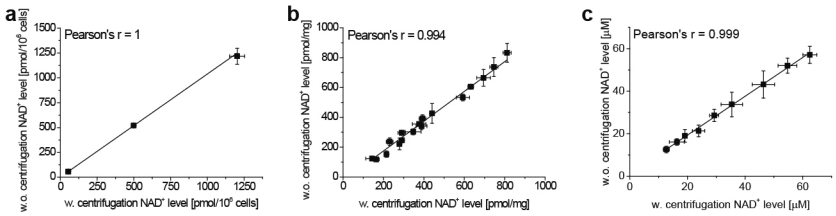

Extended Data Fig. 5 | NAD⁺ quantification by test paper for samples prepared with and without centrifugation step. a, cell lysate, **b**, homogenized mice liver and **c**, spiked human blood. Error bars represent ± SD of n = 3 independent measurements.

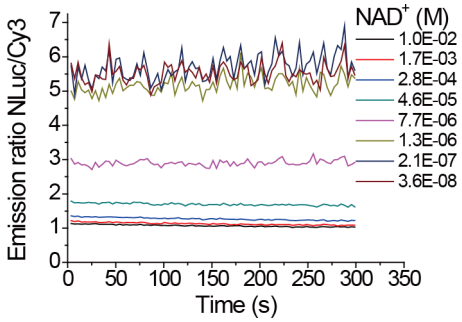

Extended Data Fig. 6 | Stability of test paper emission ratio during 5 min measurement. The ratio was monitored by camera after spotting samples with known NAD^+ concentrations onto the test paper. The stable ratio indicates a minimal sample evaporation and signal drift. The experiment was repeated three times independently with similar results.

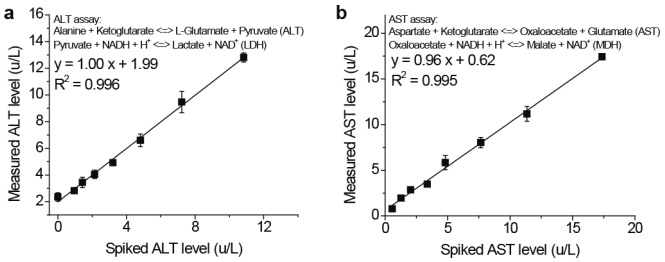

Extended Data Fig. 7 | Measurement of enzymatic activities in plasma. a, The measurement of spiked ALT in plasma. **b**, The measurement of spiked AST in plasma. Error bars represent ± SD of n = 3 independent measurements.

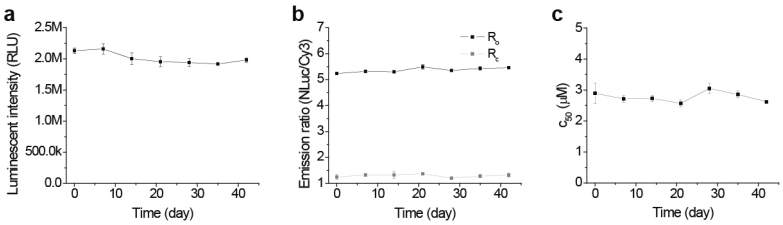

Extended Data Fig. 8 | Stability of test paper under room temperature storage. The stability is evaluated by measuring **a**, total light intensity, **b**, R_o and R_c, and **c**, c_{50}. The values were given as mean ± SD of n = 3 independent measurements.

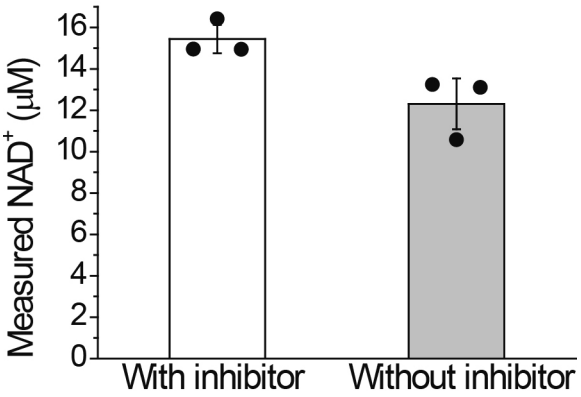

Extended Data Fig. 9 | Effect of 1 U/mL alcohol dehydrogenase (ADH from *S. cerevisiae*) on sample NAD⁺ stability. The natural level of ADH (1 U/mL) converted no more than 20% of the NAD⁺ in the sample treated using the current method compared to a method using 50 mM ADH inhibitor (4-methylpyrazole hydrochloride). Error bars represent mean ± SD of n = 3 independent measurements.

nature research

Corresponding author(s): Kai Johnsson

Last updated by author(s): Nov 2, 2019

Reporting Summary

Nature Research wishes to improve the reproducibility of the work that we publish. This form provides structure for consistency and transparency in reporting. For further information on Nature Research policies, see Authors & Referees and the Editorial Policy Checklist.

Statistics

For all statistical analyses, confirm that the following items are present in the figure legend, table legend, main text, or Methods section.

n/a	Confirmed
☐	☒ The exact sample size (*n*) for each experimental group/condition, given as a discrete number and unit of measurement
☐	☒ A statement on whether measurements were taken from distinct samples or whether the same sample was measured repeatedly
☒	☐ The statistical test(s) used AND whether they are one- or two-sided *Only common tests should be described solely by name; describe more complex techniques in the Methods section.*
☐	☒ A description of all covariates tested
☒	☐ A description of any assumptions or corrections, such as tests of normality and adjustment for multiple comparisons
☐	☒ A full description of the statistical parameters including central tendency (e.g. means) or other basic estimates (e.g. regression coefficient) AND variation (e.g. standard deviation) or associated estimates of uncertainty (e.g. confidence intervals)
☒	☐ For null hypothesis testing, the test statistic (e.g. *F*, *t*, *r*) with confidence intervals, effect sizes, degrees of freedom and *P* value noted *Give P values as exact values whenever suitable.*
☒	☐ For Bayesian analysis, information on the choice of priors and Markov chain Monte Carlo settings
☒	☐ For hierarchical and complex designs, identification of the appropriate level for tests and full reporting of outcomes
☐	☒ Estimates of effect sizes (e.g. Cohen's *d*, Pearson's *r*), indicating how they were calculated

Our web collection on statistics for biologists contains articles on many of the points above.

Software and code

Policy information about availability of computer code

Data collection	The data were collected using Tecan SparkControl™ 2.2 software, Tecan i-control™ Software, Sciex's Analyst 1.6.3 software, UVProbe Multifunctional UV Control Software, and Microsoft Excel 365. The custom code used for analyzing photos is available through this link (Kinetic/analyse/master.js): https://script.epfl.ch/script/HD/Login/ONYyswFVpd?path=test%40patiny.com%2FResearch%2FLIP
Data analysis	The data were analyzed using commercial software Sciex's MultiQuant 3.0.2, Microsoft Excel 365 and Origin 8.0. The custom code used for analyzing photos is available through this link (Kinetic/analyse/master.js): https://script.epfl.ch/script/HD/Login/ONYyswFVpd?path=test%40patiny.com%2FResearch%2FLIP

For manuscripts utilizing custom algorithms or software that are central to the research but not yet described in published literature, software must be made available to editors/reviewers. We strongly encourage code deposition in a community repository (e.g. GitHub). See the Nature Research guidelines for submitting code & software for further information.

Data

Policy information about availability of data

All manuscripts must include a data availability statement. This statement should provide the following information, where applicable:

- Accession codes, unique identifiers, or web links for publicly available datasets
- A list of figures that have associated raw data
- A description of any restrictions on data availability

The data that support the findings of this study are available from the corresponding author upon request.

Field-specific reporting

Please select the one below that is the best fit for your research. If you are not sure, read the appropriate sections before making your selection.

☒ Life sciences ☐ Behavioural & social sciences ☐ Ecological, evolutionary & environmental sciences

For a reference copy of the document with all sections, see nature.com/documents/nr-reporting-summary-flat.pdf

Life sciences study design

All studies must disclose on these points even when the disclosure is negative.

Sample size	No sample-size calculation was performed. The conventional sample size for pilot animal studies was used in this study.
Data exclusions	No data were excluded from the analysis.
Replication	For the reported data, all measurements using instruments and sensors were repeated 3 times. All attempts at replication were successful.
Randomization	All C57BL/6J male mice involved in the study were considered equal before group allocation. The mice were then allocated randomly into experimental groups. The plasma samples were collected randomly after arriving at the Clinical Chemistry Laboratory of University Hospital of Lausanne.
Blinding	The investigators were blinded to group allocation during data collection and analysis.

Reporting for specific materials, systems and methods

We require information from authors about some types of materials, experimental systems and methods used in many studies. Here, indicate whether each material, system or method listed is relevant to your study. If you are not sure if a list item applies to your research, read the appropriate section before selecting a response.

Materials & experimental systems

n/a	Involved in the study
☒	☐ Antibodies
☐	☒ Eukaryotic cell lines
☒	☐ Palaeontology
☐	☒ Animals and other organisms
☐	☒ Human research participants
☒	☐ Clinical data

Methods

n/a	Involved in the study
☒	☐ ChIP-seq
☒	☐ Flow cytometry
☒	☐ MRI-based neuroimaging

Eukaryotic cell lines

Policy information about cell lines

Cell line source(s)	HEK-293 cell were obtained from DSMZ (ACC 305)
Authentication	The cells were cultured directly from the received product. No further authentication was performed.
Mycoplasma contamination	All cell lines were tested negative for mycoplasma contamination.
Commonly misidentified lines (See ICLAC register)	None.

Animals and other organisms

Policy information about studies involving animals; ARRIVE guidelines recommended for reporting animal research

Laboratory animals	C57BL/6J male mice, 8 weeks of age.
Wild animals	The study did not involve wild animals.
Field-collected samples	The study did not involve samples collected from the field.
Ethics oversight	All animal experiments were carried according to national Swiss and European Union ethical guidelines and approved by the local animal experimentation committee of the Canton de Vaud under license #2465.

Note that full information on the approval of the study protocol must also be provided in the manuscript.

Human research participants

Policy information about studies involving human research participants

Population characteristics	No preset population characteristics were used when collecting plasma samples. As the study aims to compare two methods for quantifying plasma lactate dehydrogenase levels, 0,5 mL of patient plasma samples arriving at the Clinical Chemistry Laboratory of University Hospital of Lausanne were selected randomly without any preset criteria. All information regarding the patients from whom the plasma samples were collected were kept confidential from the experimenter.
Recruitment	The study does not involve patient recruitment. Plamsa samples without patient information were collected randomly after arriving at the Clinical Chemistry Laboratory of University Hospital of Lausanne.
Ethics oversight	University Hospital of Lausanne

Note that full information on the approval of the study protocol must also be provided in the manuscript.